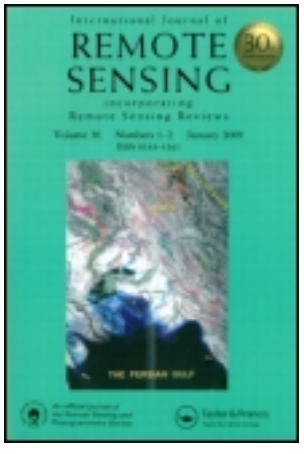

International Journal of Remote Sensing

Publication details, including instructions for authors and subscription information:
http://www.tandfonline.com/loi/tres20

Analyses of aerosol properties in Hefei based on polarization measurements of a sun photometer

Jiacheng Wang [a b c], Shizhi Yang [a b], Qiang Zhao [a b] & Shengcheng Cui [a b]

[a] Remote Sensing Laboratory, Anhui Institute of Optics and Fine Mechanics, Chinese Academy of Sciences, HeFei, 230031, PR China

[b] Key Lab of General Optical Calibration and Characterization Techniques, Chinese Academy of Sciences, HeFei, 230031, PR China

[c] College of Physics and Electronic Information, FuYang University, FuYang, 236041, PR China

Version of record first published: 24 Oct 2011.

To cite this article: Jiacheng Wang, Shizhi Yang, Qiang Zhao & Shengcheng Cui (2012): Analyses of aerosol properties in Hefei based on polarization measurements of a sun photometer, International Journal of Remote Sensing, 33:1, 69-80

To link to this article: http://dx.doi.org/10.1080/01431161.2011.562254

International Journal of Remote Sensing
Vol. 33, No. 1, 10 January 2012, 69–80

Taylor & Francis
Taylor & Francis Group

Analyses of aerosol properties in Hefei based on polarization measurements of a sun photometer

JIACHENG WANG*†‡§, SHIZHI YANG†‡, QIANG ZHAO†‡ and SHENGCHENG CUI†‡

†Remote Sensing Laboratory, Anhui Institute of Optics and Fine Mechanics, Chinese Academy of Sciences, HeFei 230031, PR China

‡Key Lab of General Optical Calibration and Characterization Techniques, Chinese Academy of Sciences, HeFei 230031, PR China

§College of Physics and Electronic Information, FuYang University, FuYang 236041, PR China

(*Received 24 March 2010; in final form 21 October 2010*)

Data collected with a CIMEL CE-318 sun-tracking photometer in Hefei between 2006 and 2008 were collected and inverted using an algorithm which takes polarization information into account. The aerosol optical depths (AOD) showed a pronounced temporal trend, with a maximum value of 0.55 at 440 nm in spring, and values around 0.45 in the remaining seasons. The Ångström parameter for all seasons exceeds 0.80 even in spring. Size distribution showed that both fine and coarse aerosol fractions change significantly and periodically in magnitude and shape during a year. Geometric mean radii for fine and coarse modes are 0.18 μm (standard deviation is 0.016) and 2.7 μm (standard deviation is 0.37), respectively. The spectral dependence of single scattering albedo and reflective index is distinct in the four seasons due to the different aerosol components. All these properties are reported, and it is expected that these aerosol characterizations will help refine aerosol models and clarify the mechanisms of aerosol radiative forcing.

1. Introduction

Atmospheric aerosol parameters are important for various applications including satellite remote sensing and computations of radiative forcing (Smirnov *et al.* 2002, Tzanis and Varotsos 2008, Zhao *et al.* 2009). Monitoring of atmospheric aerosols is a fundamentally difficult problem (Dubovik *et al.* 2002). First, compared to atmospheric gases, aerosols are highly inhomogeneous and variable; that is, aerosol observations have to be global and continuous. For instance, Varotsos *et al.* (2006), by applying detrended fluctuation analysis to the zonal mean daily Aerosol Index (AI) values derived from satellite observations during 1979–2003, showed that, globally, AI fluctuations in both hemispheres obey persistent long-range power-law correlations for time scales longer than about 4 days and shorter than about 2 years. This suggests that the AI fluctuations in small time intervals are related to the AI fluctuations in longer time intervals in a power-law fashion (when the time intervals vary from about 4 days to about 2 years). In other words, an anomaly in AI in one time

*Corresponding author. Email: shanqiangw@yahoo.com.cn

International Journal of Remote Sensing
ISSN 0143-1161 print/ISSN 1366-5901 online © 2012 Taylor & Francis
http://www.tandf.co.uk/journals
http://dx.doi.org/10.1080/01431161.2011.562254

frame continues into the next, exhibiting a power-law evolution. In addition, analysis performed on the surface aerosol particle measurements made in Athens and Baltimore revealed persistent long-range power-law correlations from about 4 hours to 9 months for PM_{10} in Athens, and lag times from about 4 hours to 2 weeks for $PM_{2.5}$ fluctuations in a 6-month data set collected in East Baltimore (Varotsos *et al.* 2005). Second, the available accuracy of aerosol characterization is often not sufficient. In spite of high temporal and spatial aerosol variability, there are a rather limited number of general categories of aerosol types with distinctly different properties, such as (1) urban-industrial aerosols from fossil fuel combustion in populated industrial regions; (2) biomass-burning aerosols produced by forest and grassland fires; (3) desert dust blown into the atmosphere by wind; and (4) aerosols of marine origin (Dubovik *et al.* 2002, Varotsos 2005, Ferm *et al.* 2006). Ground-based aerosol remote sensing does not provide global coverage; however, its wide angular and spectral measurements of solar and sky radiation are best suited to reliably and continuously derive the detailed aerosol characteristics in key locations. Moreover, some instruments have polarization channels, which can add more information in retrieval process. The Aerosol Robotic Network (AERONET) (Holben *et al.* 1998) comprises more than 400 sites located in cities, islands, deserts and forest or grassland worldwide. So the aerosol data collected by AERONET are very useful in clarifying the mechanisms of aerosol radiative forcing and refining aerosol models.

Hefei, an AERONET site, is located in central China. The transitions of four seasons are very clear: winter (December–February), spring (March–May), summer (June–August) and autumn (September–November). In winter, winds are mainly from the northwest, bringing dry air and some dust; while in spring, winds are predominantly from the east, with the highest speeds of the year, and bring dust and sea-salt particles from land and ocean. The summer is hot and rainy. The autumn is sunny and often influenced by northerly airstreams. Aerosols there exhibit the typical urban-industrial aerosol properties of central China.

The instrument in Hefei is an automatic sun and sky scanning sun photometer, which measures the direct sun and diffuse sky radiances. Then, the aerosol properties are retrieved by using the updated inversion algorithm developed by Dubovik *et al.* (2006). Compared to the original algorithm, this version models aerosols as a mixture of spherical and non-spherical aerosol components and provides the fraction of spherical particles as an additional retrieval parameter. The non-spherical component is modelled by a mixture of randomly oriented spheroids tuned to fit laboratory polarimetric measurements of desert dust. It also should be noted that the new algorithm allows fitting not only the measurements of the total radiance but also polarization, which is sensitive to aerosol optical and microphysical properties (Li *et al.* 2009). To ensure the obtaining of reliable data, the instrument was regularly calibrated in collaboration with LOA-PHOTONS (Laboratoire d'Optique Atmosphérique, Centre National de la Recherche Scientifique, France) (Xianhua *et al.* 2008). The calibration includes three parts: the calibration of direct-sun measurements, the calibration of radiance measurements and the calibration of polarization measurements. After these calibrations, the measurement uncertainty is about 0.01–0.02 in the aerosol optical depth, about 2–4% in the radiance and about 0.0085 in the degree of linear polarization (DOLP). The information and results of the calibrations are shown in figure 1.

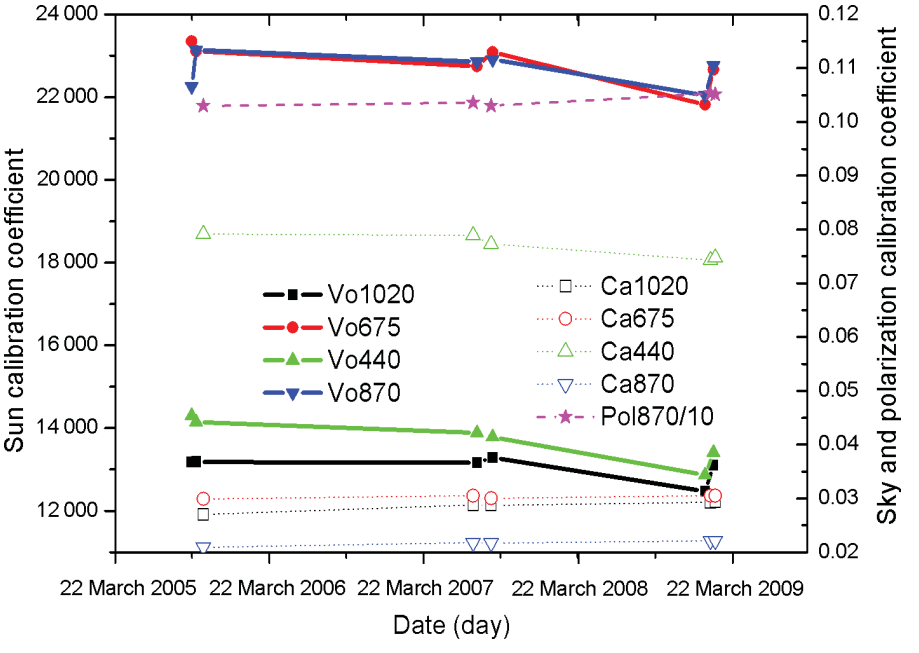

Figure 1. The information and results of calibration.

2. Measurements

Li *et al.* (2009) have shown that multi-wavelength polarization measurements nearly double the input information of aerosol retrievals thus providing a unique opportunity for aerosol inversion. The type of instrument in Hefei is the CE-318, which provides a single polarization channel centred at 870 nm. All the measurements (including polarization measurements) have been used in retrieving aerosol properties. We find that, although only one channel polarization measurement has been added in the retrieval process, the retrieved parameters also show some different characteristics (figure 2). Similar to the inversion products of multi-wavelength polarization measurements, the inversion products of single-wavelength polarization measurements also exhibit several important tendencies, as shown in figure 2.

1. The measurements of DOLP depend on aerosol models. The value of measured DOLP is high when the aerosol is dominated by fine particles or coarse spherical particles or mixed aerosol (both coarse and fine mode aerosols are presented) as shown in figure 2(*a*)–(*c*). But the DOLP is low when the aerosol is dominated by coarse non-spherical particles, figure 2(*d*).
2. Polarization measurements can help correct the underestimation of the real part of the refractive index n_r and overestimation of the fine mode size distribution when the aerosol is dominated by fine particles or mixed fine and coarse modes (the first and third row of figure 2).
3. In the case of aerosol dominated by coarse spherical particles (the second row of figure 2), polarization can help correct the overestimation of the real part of the refractive index n_r and the coarse mode size distribution.

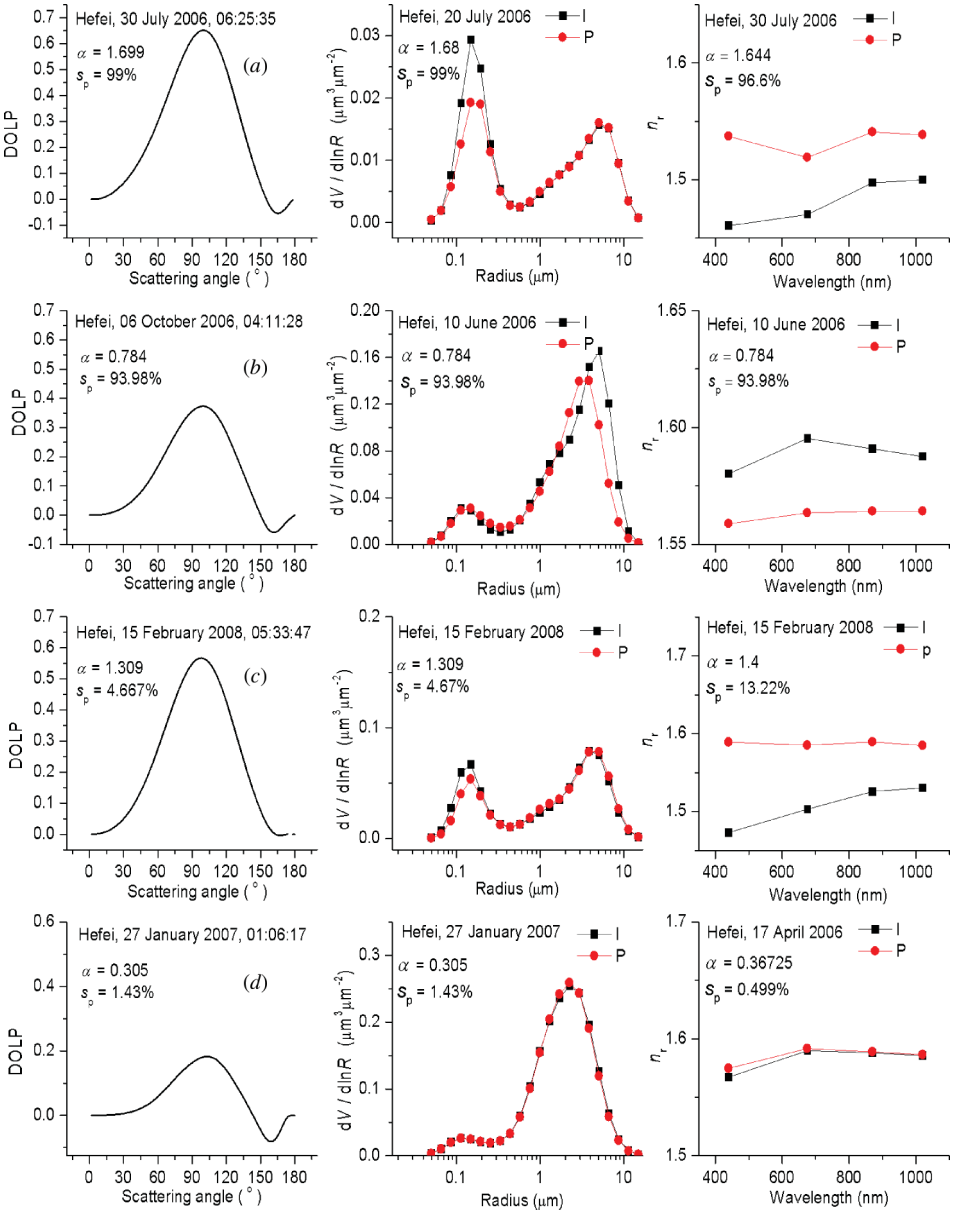

Figure 2. Examples of CE-318 measurements (DOLP – degree of linear polarization of sky light) and the retrieved aerosol properties. dV/dln$R$, particle size distribution; α Ångström parameter; s_p, fraction of spherical aerosol component; n_r, real part of refractive index.

4. In the case of aerosol dominated by coarse non-spherical particles (the last row of figure 2), there is nearly no difference between inversion products derived from intensity-only (I) and polarization-intensity (P).

For the reason above, the polarization-intensity inversion products were used in analysing aerosol optical and microphysical properties in Hefei.

3. Results

3.1 *Aerosol optical depth and Ångström parameter*

Atmospheric aerosol optical conditions can be characterized by two parameters: optical depth and Ångström parameter. Figure 3(*a*) and (*b*) illustrate the monthly averaged aerosol optical depth at 440 nm and the Ångström parameter in Hefei respectively. Generally, the monthly averaged aerosol optical depth shows higher values from February to June, then gives the lowest value in July, and holds middle values from August to November, finally decreasing to lower values in December and January. Different from the variety of optical depth, the Ångström parameter shows lower values from February to June, then gives the highest value in July, holds higher values from August to November, and finally decreases to lower values in December and January. The temporal varieties of AOD and Ångström in Hefei are closely related to the following factors. (1) Rain, which can remove aerosols by the processes of rainout, washout and sweepout. These removal mechanisms are all very efficient at depositing coarse particles (Chate *et al.* 2003). (2) Wind, which can bring in and take away aerosol particles (Smirnov *et al.* 2002, Zhao *et al.* 2008). (3) Humidity, which can influence the size of some aerosol particles (Shettle and Fenn 1979). Specifically, first, less rainfall, low vegetation cover and high speed wind result in the increase of dust in the air from February to May, and this would cause an increase in aerosol optical depth

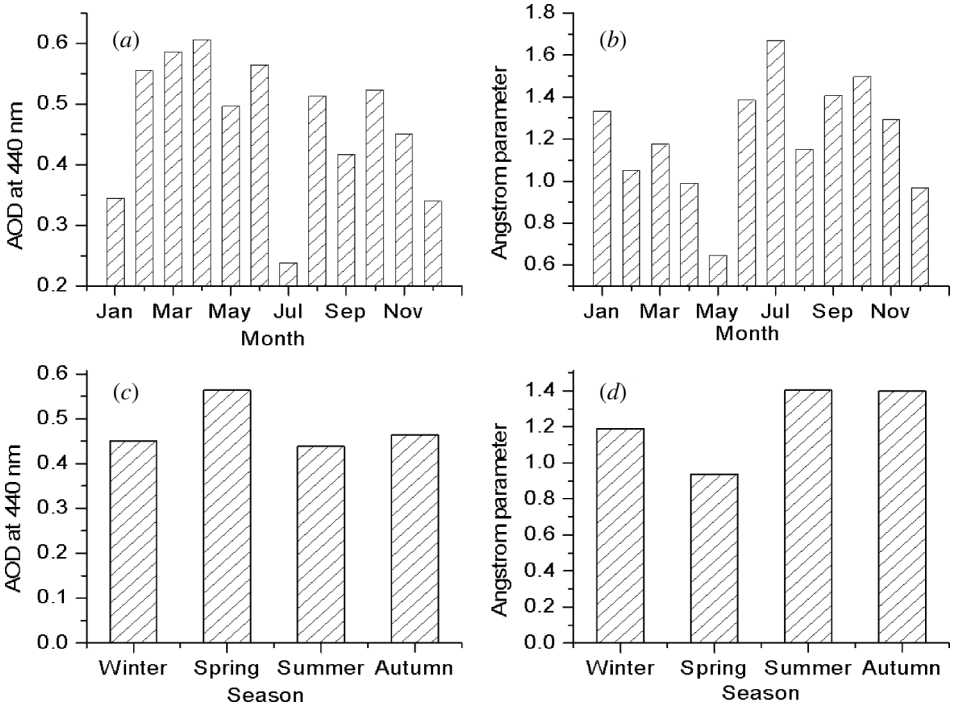

Figure 3. Relationship between corrected microwave-derived air temperature ($T_a c$) and measured air temperature from an independent database. (*a*) Monthly averaged AOD at 440 nm; (*b*) monthly averaged Ångström parameter; (*c*) seasonal averaged AOD at 440 nm; (*d*) seasonal averaged Ångström parameter.

and a decrease in Ångström parameter (Chun *et al.* 2001, Huebert *et al.* 2003, Eck *et al.* 2005). Second, July is the "plum rain season" in Hefei, and rainout efficiency results in the minimum aerosol optical depth and the highest Ångström parameter (Chate *et al.* 2003). Third, due to the stability of the atmosphere from August to November, aerosols are mainly dominated by fine particles produced by industry productivities, and this would result in a higher Ångström parameter (Dubovik *et al.* 2002). Finally, in December and January, cold wind brings some dust and carries away some fine particles, and this would result in lower values of aerosol optical depth and Ångström parameter. Some of the results are similar to the results reported by Eck *et al.* (2005). Seasonal averaged aerosol optical depth at 440 nm and Ångström parameter are shown in figure 3(*c*) and (*d*), respectively. The maximum aerosol optical depth appears in spring. The remaining seasons have nearly the same value, around 0.45. The yearly averaged AOD at 440 nm is 0.4789. The maximum and minimum Ångström parameter are 1.64 and 0.65 respectively. This means that the particle size distribution varies strongly in a year.

3.2 *Particle size distribution*

Aerosol particle size distribution was retrieved from spectral sun and sky radiance data by an iterative algorithm. The inversion algorithm produces retrievals that correspond to the effective optical and microphysical properties for the total atmospheric column. According to Dubovik, non-spherical dust aerosols can be retrieved reasonably well when the angular range of sky radiances is limited to scattering angles smaller than 30°–40°. So the polarization-intensity data acquired around midday (scattering angle range is small) was selected to analyse aerosol size distributions (Dubovik *et al.* 2000).

Figures 4 and 5 illustrate monthly and seasonal averaged size distributions ($\mathrm{d}V/\mathrm{d}\ln R$), respectively. Clearly they agree with the bimodal lognormal volume size distributions very well. Both fine and coarse modes show relative stability and display relatively smooth shapes. The variation of the amplitude of the two modes exhibits an obvious periodicity in a year. Generally, aerosols are dominated by fine particles in summer and autumn, and coarse particles in spring and winter. This means that fine particles are not always the dominant component in urban areas all year. This can be attributed to the difference of incoming coarse particles in different seasons. In spring, winds are mainly from east or west with the highest speed in a year removing parts of small particles and bringing large particles (such as dust from land and sea salt from ocean). During winter, winds are mainly from the northwest, bringing dust and removing some small particles. In summer and autumn, fine particles become the dominant component in aerosols over Hefei due to little effect of winds. It also should be noted that both fine and coarse aerosol fractions change significantly and periodically in the magnitude and shape of size distribution during a year.

Table 1 presents parameters of the bimodal lognormal volume size distributions (Remer *et al.* 1999, Whitby 1978) shown in figures 4 and 5. For each mode the log normal distribution is defined as:

$$\frac{\mathrm{d}V}{\mathrm{d}\ln R} = \frac{C_\mathrm{v}}{\sigma\sqrt{2\pi}} \exp\left[-\frac{1}{2}\left(\frac{\ln(R/R_\mathrm{v})}{\sigma}\right)^2\right], \tag{1}$$

where $\mathrm{d}V/\mathrm{d}\ln R$ is the volume distribution, the volume concentration C_v is the columnar volume of particles per unit cross section of atmospheric column, σ is the standard

Table 1. Parameters of aerosol particle size distribution over Hefei.

	Fine mode				Coarse mode			
	C_v ($\mu m^3 \mu m^{-2}$)	R_{eff}(μm)	R_v(μm)	σ	C_v ($\mu m^3 \mu m^{-2}$)	R_{eff}(μm)	R_v(μm)	σ
January	0.0562	0.1609	0.1806	0.4819	0.1782	2.2844	2.7757	0.6158
February	0.1126	0.1662	0.1912	0.5335	0.1019	2.1866	2.6540	0.6239
March	0.0664	0.1438	0.1637	0.5080	0.2021	1.8834	2.2957	0.6261
April	0.0547	0.1484	0.1673	0.4930	0.2000	1.8370	2.2998	0.6744
May	0.0525	0.1700	0.1975	0.5355	0.1497	1.5628	1.8790	0.6075
June	0.0992	0.1744	0.1986	0.5017	0.0965	2.3028	2.9159	0.6851
July	0.0235	0.1581	0.1741	0.4437	0.0288	2.5011	3.3353	0.7390
August	0.1540	0.1830	0.2090	0.5190	0.0715	2.3650	2.8350	0.6120
September	0.0990	0.1678	0.1903	0.5073	0.0230	2.2921	2.7558	0.6145
October	0.0898	0.1561	0.1726	0.4637	0.0697	2.1715	2.7856	0.7125
November	0.0662	0.1438	0.1621	0.5095	0.0729	2.3286	2.8360	0.6201
December	0.0608	0.1414	0.1625	0.5370	0.1093	2.1511	2.8075	0.7204
Mean	0.0779	0.1595	0.1808	0.5028	0.1086	2.1555	2.6813	0.6543
S_{td}	0.0347	0.0133	0.0161	0.0287	0.0616	0.2660	0.3705	0.0488
V_{ar}	0.4448	0.0836	0.0892	0.0572	0.5667	0.1234	0.1382	0.0746

Note: C_v is the volume concentration; R_{eff} the effective radius; R_v the volume geometric mean radius; σ the geometric standard deviation; S_{td} denotes statistical standard deviation of the four parameters between 2006 and 2008; V_{ar} denotes variation coefficient of the four parameters between 2006 and 2008.

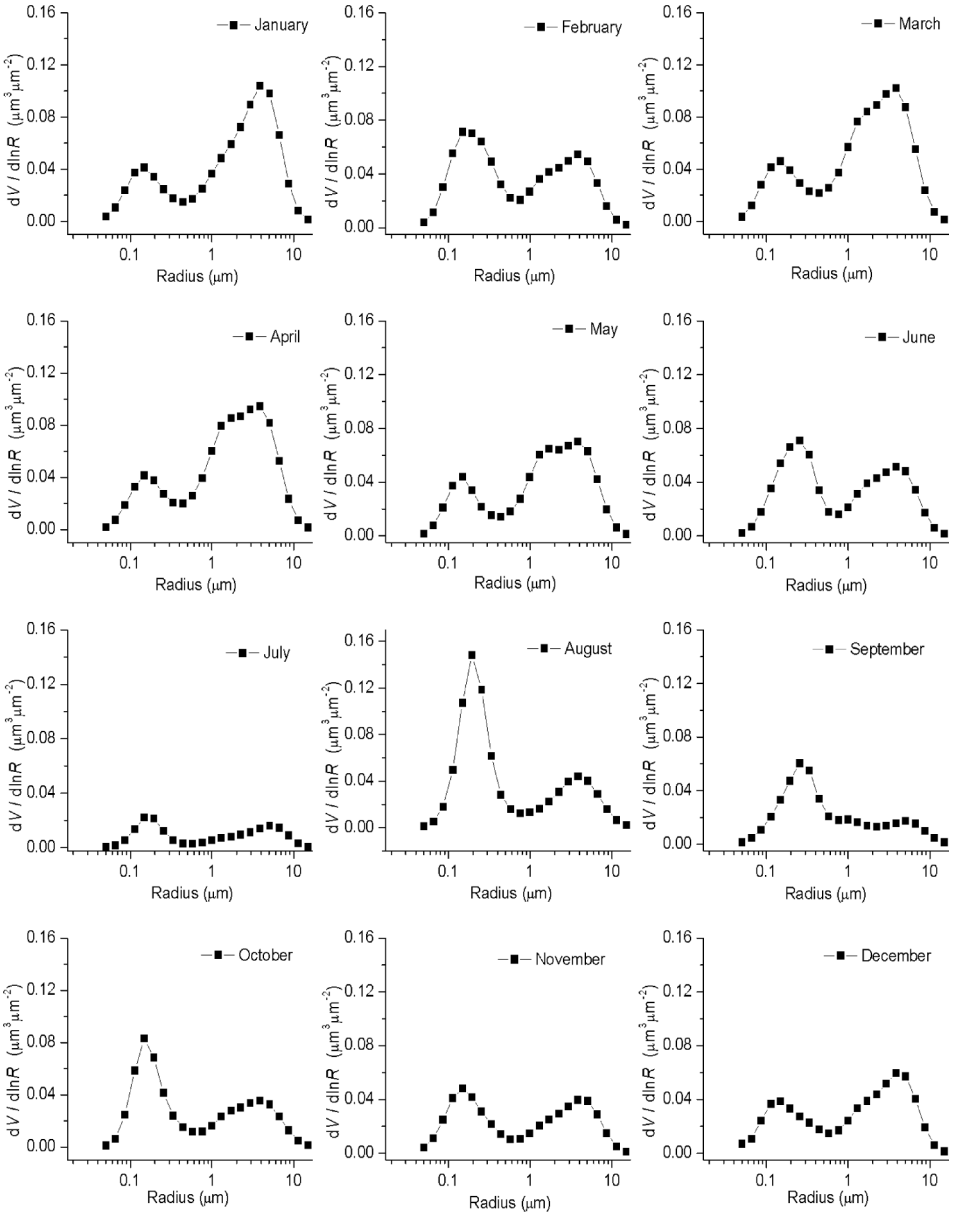

Figure 4. Monthly averaged particle size distribution.

deviation (SD) of ln R, that is, $\sigma^2 =< (\ln R - \ln R_v)^2 >$, R is the particle radius and R_v is the volume geometric mean radius. As usual, we assigned particles with radii $0.05 < R < 0.6$ μm and with radii $0.6 < R < 15$ μm to the fine and coarse modes, respectively. Effective radius (defined as a ratio of the third over the second moment of the number size distribution) for each fraction is also presented in table 1.

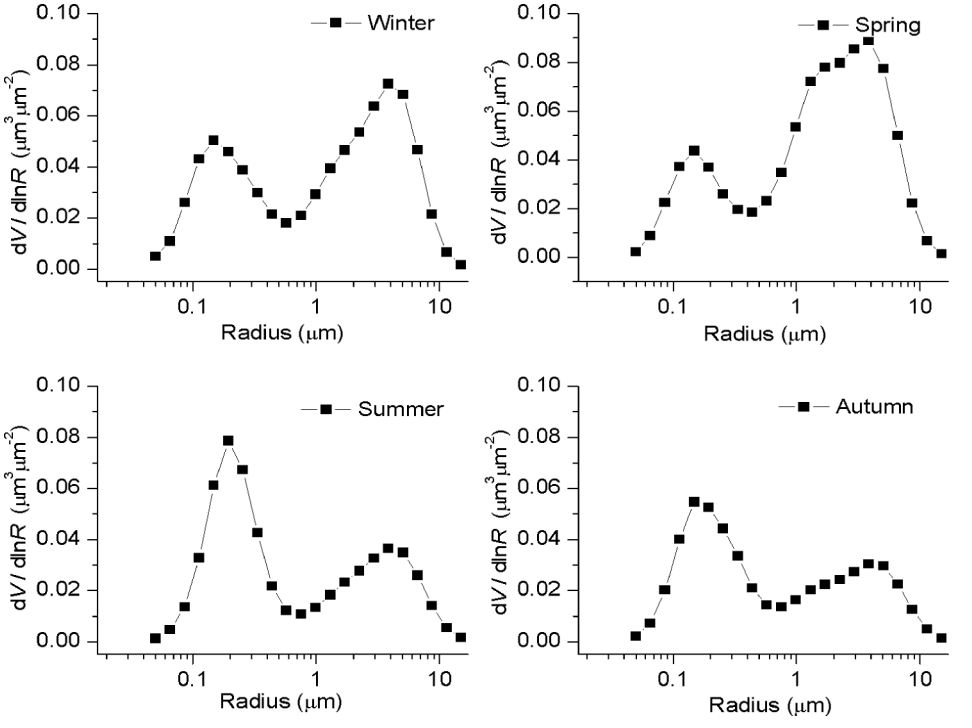

Figure 5. Seasonal averaged particle size distribution.

The annual averaged article volume concentrations for fine and coarse modes are very close: for fine mode, mean volume concentration is 0.0779, standard deviation 0.0347; for coarse mode, mean volume concentration is 0.1086, standard deviation 0.0616. The annual averaged particle geometric mean radii for fine and coarse modes are 0.18 μm (SD 0.016) and 2.7 μm (SD 0.37), respectively. Variation coefficients (defined as standard deviation divided by average) yielded values of 8.92% for the fine mode R_v and 5.72% for the fine mode σ, and 13.82% and 7.46% for the coarse mode parameters (table 1).

3.3 *Single scattering albedo and refractive index*

The analysis showed that an accurate single scattering albedo (SSA) retrieval (with accuracy to the level of 0.03) and complex index of refraction (errors on the order of 30%–50% for the imaginary part of the refractive index n_i and 0.04 for the real part of the refractive index n_r) can be retrieved only for high aerosol loading (AOD at 440 nm larger than 0.5) for solar zenith angle $> 50°$ (i.e. the range of scattering angles in measured solar almucantar $> 100°$). For observations with lower aerosol loading, the retrieval accuracy of SSA, n_i and n_r significantly decreases because of the decrease of the information content (Dubovik *et al.* 2002). Thus the early morning or late afternoon measurements with high aerosol optical depth are selected for analysing SSA and refractive index.

The seasonal averaged SSA retrieved from the whole period of observations is shown in figure 6(*a*). Several major features can be observed. First, averaged seasonal

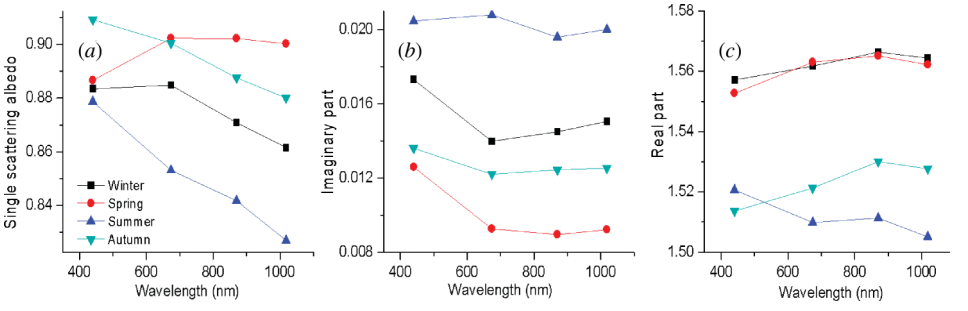

Figure 6. Seasonal averaged single scattering albedo and refractive index.

SSA is less than 0.92 at all the four bands (440, 670, 870, 1020 nm) in four seasons, especially in winter and summer, the values are less than 0.89. This means that aerosols in Hefei absorb a little strongly. Second, SSA shows an obvious spectral dependence except for in winter. SSA decreases with wavelength in summer and autumn because aerosols are dominated by fine particles produced by anthropogenic combustion processes from the use of fossil fuels and the absorption properties of these particles can cause the spectral dependence of SSA. In spring, SSA has higher values and the values increase from the blue to the red spectral bands. This is because dust and salt are the major contributors to the atmospheric optical state; these coarse particles absorb less than the anthropogenically influenced aerosols (Levin *et al.* 1980) and have a relatively strong absorption in the blue spectral band (Kaufman *et al.* 2001). Third, SSA exhibits significant difference between winter and spring, even though the particle size distribution is similar in the two seasons. This difference may result from increasing combustion of coal in winter.

Averaged seasonal aerosol refractive indices over Hefei are shown in figure 6(*b*) and (*c*). The indices of refraction are not independent from the single scattering albedo and size distribution. First, higher SSA is somewhat correlated with the lower imaginary part of the refractive index, and vice versa. This correlation is expected because, in the Mie formalism, the imaginary part predetermines the absorption of light by small particles (while the SSA also depends on particle size). Such correlation can be seen clearly in figure 6(*a*) and (*b*). Second, in winter, spring and summer, higher SSA correlates to a higher real part of the refractive index, and vice versa. This tendency agrees with the electromagnetic theory (Bohren and Huffman 1983) that the total scattering increases with an increase of the real part. But in autumn, higher SSA is correlated with a lower real part of the refractive index. According to Dubovik *et al.* (2002), this kind of correlation is likely to be due to the higher relative humidity and resultant aerosol hygroscopic growth.

4. Conclusions

Analyses of aerosol optical properties were performed, and the principal conclusions drawn from our work can be summarized as follows.

1. The annual cycle of seasonal mean AOD and Ångström parameter show maximum and minimum values in spring because of the influence of the maximum dust-storm activity in China in this season. However, the minimum Ångström parameter for all seasons exceeds 0.80 even in spring, suggesting that while dust

contributions to total aerosol optical depth are significant, fine mode aerosol contributes more to the optical depth during the entire year.

2. Column integrated volume size distribution over Hefei shows a periodic variability in a year. In spring and winter, coarse particles are the dominant component, while in summer and autumn, the case is reversed.
3. The spectral dependence of SSA is different throughout the year. In spring, SSA increases with wavelength because dust is the major component. In summer and autumn, SSA decreases with wavelength due to urban fine particles being the dominant component. This decreasing spectral trend is similar to the results obtained by Dubovik *et al.* (2002) for urban pollution and smoke aerosols. The spectral variability of SSA is very complex in winter. The aerosol refractive index is not independent from SSA and size distribution. Higher SSA correlates to a lower imaginary part and a higher real part of the refractive index. But some exceptions appear in autumn because the real part of the refractive index can also be influenced by humidity in the atmosphere.

Acknowledgments

We would like to thank Yanli Qiao and Zhengqiang Li. for their efforts in establishing and maintaining the Hefei site. We also thank Zhengqiang Li for providing inversion products retrieved from both intensity and polarization data. This work was funded by the project of Chinese Academy of Science numbered INFO-115-C01-SDB4-27, the project of 973 numbered 2010CB950800 and the Knowledge Innovation Programme of the Chinese Academy of Sciences Programme through grant number 083RC11125.

References

Bohren, C.F. and Huffman, D.R., 1983, *Absorption and scattering of light by small particles*, p. 550 (New York: John Wiley and Sons).

Chate, D.M., Rao, P.S.P., Naik, M.S., Momin, G.A., Safai, P.D. and Ali, K., 2003, Scavenging of aerosols and their chemical species by rain. *Journal of Atmospheric Environment*. *37*, pp. 2477–2484.

Chun, Y., Boo, K.-O., Kim, J., Park, S.-U. and Lee, M., 2001, Synopsis, transport, and physical characteristics of Asian dust in Korea. *Geophysical Research*, **106**, pp. 18461–18469.

Dubovik, O., Holben, B.N., Eck, T.F., Smirnov, A., Kaufman, Y.J., King, M.D., Tanré, D. and Slutsker, I., 2002, Variability of absorption and optical properties of key aerosol types observed in worldwide locations. *Journal of the Atmospheric Sciences*, **59**, pp. 590–608.

Dubovik, O., Sinyuk, A., Lapyonok, T., Holben, B.N., Mishchenko M., Yang P. and Eck, T.F., 2006, Application of spheroid models to account for aerosol particle nonsphericity in remote sensing of desert dust. *Geophysical Research*, **111**, D11208 doi:10.1029/2005JD006619.

Dubovik, O., Smirnov, A., Holben, B.N., King, M.D., Kaufman, Y.J., Eck, T.F. and Slutsker, I., 2000, Accuracy assessments of aerosol optical properties retrieved from AERONET sun and sky-radiance measurements. *Geophysical Research*, **105**, pp. 9791–9806.

Eck, T.F., Holben, B.N., Dubovik, O., Smirnov, A., Goloub, P., Chen, H.B., Chatenet, B., Gomes, L., Zhang, X.Y., Tsay, S.C., Ji, Q., and Slutsker, I., 2005, Columnar aerosol optical properties at AERONET sites in central eastern Asia and aerosol transport to the tropical mid-Pacific. *Geophysical Research*, **110**, D06202 doi:10.1029/2004JD005274.

Ferm, M., Watt, J., O'Hanlon, S., Desantis, F. and Varotsos, C., 2006, Deposition measurement of particulate matter in connection with corrosion studies. *Analytical and Bioanalytical Chemistry*, **384**, pp. 1320–1330.

Holben, B.N., Eck, T.F., Slutsker, I., Tanré, D., Buis, J.P., Setzer, A., Vermote, E., Reagan, J.A., Kaufman, Y.J., Nakajima, T., Lavenu, F., Jankowiak, I. and Smirnov, A., 1998, AERONET: a federated instrument network and data archive for aerosol characterization. *Remote Sensing of Environment*, **66**, pp. 1–16.

Huebert, B.J., Bates, T., Russell, P.B., Shi, G., Kim, Y.J., Kawamura, K., Carmichael, G. and Nakajima, T., 2003, An overview of ACE-Asia: strategies for quantifying the relationships between Asian aerosols and their climatic impacts. *Geophysical Research*, **108**, 8633.

Kaufman, Y.J., Tanré, D., Dubovik, O., Karnieli, A. and Remer, L.A., 2001, Absorption of sunlight by dust as inferred from satellite and ground based remote sensing. *Geophysical Research Letters*, **28**, pp. 1479–1483.

Levin, Z., Joseph, J.H. and Mekler, Y., 1980, Properties of Sharav (Khamsin) dust: comparison of optical and direct sampling data. *Journal of the Atmospheric Sciences*, **37**, pp. 882–891.

Li, Z., Goloub, P., Dubovik, O., Blarel, L., Zhang, W.X., Podvin, T., Sinyuk, A., Sorokin, M., Chen, H.B., Holben, B.N., Tanré, D., Canini, M. and Buis, J.P., 2009, Improvements for ground-based remote sensing of atmospheric aerosol properties by additional polarimetric measurements. *Journal of Quantitative Spectroscopy & Radiative Transfer*, **110**, pp. 1954–1961.

Remer, L.A., Kaufman, Y.J. and Holben, B.N., 1999, Interannual variation of ambient aerosol characteristics on the east coast of the United States. *Geophysical Research*, **104**, pp. 2223–2231.

Shettle, E.P. and Fenn. R.W., 1979, *Models for the aerosols of the lower atmosphere and the effects of humidity variations on their optical properties*, Report. Tr-79-0214 (Hanscom Air Force Base, MA: US Air Force Geophysics Laboratory).

Smirnov, A., Holben, B.N., Dubovik, O., O'Neill, N.T., Eck, T.F., Westphal, D.L., Goroch, A.K., Pietras, C. and Slutsker, I., 2002, Atmospheric aerosol optical properties in the Persian Gulf. *Journal of the Atmospheric Sciences*, **59**, pp. 620–634.

Tzanis, C. and Varotsos, C.A., 2008, Tropospheric aerosol forcing of climate: A case study for the greater area of Greece. *International Journal of Remote Sensing*, **29**, pp. 2507–2517.

Varotsos, C., 2005, Airborne Measurements of aerosol, ozone, and solar ultraviolet irradiance in the troposphere. *Journal of Geophysical Research-Atmospheres*, **110** (D09202 doi:10.1029/2004JD005397.

Varotsos, C., Ondov, J. and Efstathiou, M., 2005, Scaling properties of air pollution in Athens, Greece and Baltimore, Maryland. *Atmospheric Environment*, **39**, pp. 4041–4047.

Varotsos, C.A., Ondov, J.M., Cracknell, A.P., Efstathiou, M.N. and Assimakopoulos, M.N., 2006, Long-range persistence in global Aerosol Index dynamics. *International Journal of Remote Sensing*, **27**, pp. 3593–3603.

Whitby, K.T., 1978, The physical characteristics of sulfur aerosols. *Atmospheric Environment*, **12**, pp. 135–159.

Xianhua, W., Yanli, Q., Goloub, P. and Li, Z.Q., 2008, Radiometric calibration of sun photometer system applied to aerosol robotic network. *Acta Optica Sinica*, **28**, pp. 87–91.

Zhao, Q., Yang, S.Z., Qiao, Y.L. and Ma, J.J., 2009, Simultaneous non-linear retrieval of atmospheric profiles and surface skin temperature from MODIS infrared radiances in Taiwan Strait. *International Journal of Remote Sensing*, **30**, pp. 3027–3040.

Zhao, Q., Yang, S.Z., Qiao, Y.L. and Yuan, G.Y., 2008, Analysis of the optical characteristic of littoral aerosol influenced by typhoon. *Acta Optica Sinica*, **28**, pp. 2046–2050.